The role of soil ice in land-atmosphere coupling over the United States: A soil moisture–precipitation winter feedback mechanism

Ahmed B. Tawfik[1] and Allison L. Steiner[1]

Received 7 April 2010; revised 28 October 2010; accepted 3 November 2010; published 22 January 2011.

[1] We perform two 23 year simulations using a regional climate model coupled with the National Center for Atmospheric Research Community Land Model version 3.5 (RegCM-CLM) to investigate land-atmosphere coupling in the continental United States during the cold season (October–April) and the role of soil water phase. One simulation allows the land surface to interact freely (RunI) while the other simulation uses monthly climatological soil moisture (soil liquid plus soil ice) to represent an uncoupled land surface (RunC). A winter land-atmosphere coupling signal occurs slightly south of the freezing line, indicating that the freezing line could be regarded as a temporally varying transition zone similar to the dry-to-wet transition zone identified in prior studies during boreal summer. Warmer soil temperatures in RunI translate into additional available surface energy (sum of latent and sensible heat) producing locally elevated moist static energy in the atmosphere. Additionally, warmer temperatures and greater moist static energy increase both large-scale (6–30% increase, March) and convective precipitation (>100% increase, April). As a result of the increased liquid precipitation during transition months, soil liquid water increases thereby warming winter ground and air temperatures in the interactive run and enhancing the potential for subsequent liquid precipitation. While RunC includes more persistent soil ice than is likely present in the real land-atmosphere system, this precipitation-soil moisture feedback underscores the role of soil moisture phase and variability as an important surface parameter in the winter months.

Citation: Tawfik, A. B., and A. L. Steiner (2011), The role of soil ice in land-atmosphere coupling over the United States: A soil moisture–precipitation winter feedback mechanism, *J. Geophys. Res.*, *116*, D02113, doi:10.1029/2010JD014333.

1. Introduction

[2] The land surface can be considered the lower boundary condition to the atmosphere, and represents a key source of energy input to the atmosphere through the release of sensible and latent heat fluxes. Many variables can affect this release of energy, including the amount of incoming solar radiation, land cover type, soil properties, and soil water phase. Across many regions, soil moisture is an important determinant in both the partitioning of surface energy and the magnitude of these fluxes to the atmosphere [*Betts*, 2004; *Dirmeyer*, 2006]. This interaction between the land and the atmosphere is well documented during summer months [*Schar et al.*, 1999; *Pal and Eltahir*, 2001; *Findell and Eltahir*, 2003], but is often regarded as too weak to be important during winter [*Zhang et al.*, 2008a]. This study focuses on the impact of soil moisture and its phase on the seasonal evolution of the land-atmosphere feedback, with particular emphasis on the winter months. We find that the presence of soil ice can trigger land-atmosphere feedbacks through modifications of available surface energy, moist static energy, and convective and large-scale precipitation.

[3] Soil moisture can interact with the atmosphere on a broad range of spatial scales. At the local scale, evaporation can directly produce local precipitation [*Schar et al.*, 1999]. Additionally, moisture from remote locations can be advected into a region and amplified by local soil moisture, creating precipitation and an indirect interaction between the land surface and precipitation. The relative importance of the direct and indirect pathways can be quantified using the recycling ratio, β [*Schar et al.*, 1999]:

$$\beta = ET/(ET + IN), \tag{1}$$

where ET is evapotranspiration and IN is the moisture transported into a defined region. Previous studies have shown that an indirect mechanism tends to dominate over local precipitation recycling in most basins [*Schar et al.*, 1999; *Zhang and Frederiksen*, 2003].

[4] In addition to spatial influences, soil moisture can affect the atmosphere through a continuum of temporal scales [*Betts and Ball*, 1995; *Betts et al.*, 1996]. Typically, the concept of soil moisture "memory" on the seasonal time scale refers to the ability of soil moisture to provide some residual information of past atmospheric events. This memory occurs because soil moisture evolves at relatively

[1]Department of Atmospheric, Oceanic, and Space Sciences, University of Michigan, Ann Arbor, Michigan, USA.

0148-0227/11/2010JD014333

longer time scales than the overlying atmosphere. For example, an increase in soil moisture can produce anomalously high latent heat fluxes long after a precipitation event has occurred. Several modeling studies have found that springtime dry soil moisture anomalies tend to decrease summer rainfall [*Fennessy and Shukla*, 1999; *Pal and Eltahir*, 2001; *Kim and Wang*, 2007; *Wu et al.*, 2007]; field measurements in the central United States confirm a similar soil moisture–precipitation feedback [*Findell and Eltahir*, 1997; *Eltahir*, 1998].

[5] The relationship between land surface conditions such as soil moisture and atmospheric variables are often described with a parameter known as "coupling strength" [*Dirmeyer*, 2001; *Koster et al.*, 2002]. The coupling strength quantifies impacts of soil moisture anomalies on atmospheric variables (e.g., precipitation and surface air temperature) and describes the extent of communication between the land and the atmosphere. *Koster et al.* [2002] examined the intermodel variability and found marked differences in coupling strength between four Atmospheric General Circulation Models (AGCMs) during boreal summer. The Global Land-Atmosphere Coupling Experiment (GLACE) expanded upon this work using 12 AGCMs and identified common "hot spots" across models, generally located between dry and wet regions [*Koster et al.*, 2004; *Guo et al.*, 2006; *Koster et al.*, 2006]. Observations have further emphasized the role of soil moisture transition zones as regions with greater land-atmosphere coupling [*Zhang et al.*, 2008b]. Recent studies have explored land-atmosphere coupling using regional climate models to determine if similar coupling regimes are present with higher spatial resolution models. Using Weather Research and Forecasting (WRF), *Zhang et al.* [2008a] could not confirm the presence of a land-atmosphere hot spot as identified by GLACE over the Southern Great Plains and found coupled regions to be within a specific surface air temperature range (23°C–29°C).

[6] To date, the literature regarding land-atmosphere coupling has been focused on the feedbacks between soil moisture and atmospheric variables during boreal summer. This is under the presumption that soil moisture and local evaporative feedbacks would be less significant than synoptic-scale processes in modifying temperature and precipitation in the winter midlatitudes. While synoptic systems dominate midlatitude winter climates due to strong meridional temperature gradients [*Sickmoller et al.*, 2000; *de la Torre et al.*, 2008], the potential coupling between land and atmosphere could occur in seasons outside of boreal summer. For example, soil water phase may have strong impacts on the surface energy budget [*Viterbo et al.*, 1999; *Boone et al.*, 2000]. Limited observational studies suggest a connection between soil water phase and atmospheric processes, where reduced winter precipitation is found to promote soil freezing throughout the season when snow cover is thin [*Isard and Schaetzl*, 1998; *Henry*, 2008].

[7] Similar to reduced spring rainfall triggering summer drought, reduced winter precipitation could support more soil water freezing, cooler temperatures, and decreased surface fluxes. These modifications to surface conditions could then feedback to additional reductions in precipitation. Observational studies suggest this relationship between reduced winter precipitation and soil freezing is most pronounced for locations near the freezing line [*Isard and Schaetzl*, 1998; *Henry*, 2008], which could allow the surface freezing line to act as a transition zone analogous to the wet-dry transition zone normally associated with land-atmosphere hotspots. This study examines the seasonal evolution of land-atmosphere coupling and the role of soil water phase, and suggests a likely mechanism for winter land-atmosphere coupling. Section 2 describes the model and experiment design used in the analysis, section 3 evaluates model sensitivity of coupling strength, section 4 discusses model evaluation and present results of the experiment, and a discussion of the winter feedback mechanism is presented in section 5.

2. Methods

2.1. Description of Climate-Land Surface Model (RegCM-CLM)

[8] To evaluate land-atmosphere feedbacks, high-resolution regional climate model simulations are conducted using the Abdus Salaam International Center for Theoretical Physics (ICTP) Regional Climate Model (RegCM) coupled with the National Center for Atmospheric Research (NCAR) Community Land Model (CLM) version 3.5 [*Oleson et al.*, 2004]. RegCM is a community-based, compressible, hydrostatic, primitive-equation model [*Giorgi and Mearns*, 1999; *Pal et al.*, 2007].

[9] Large-scale precipitation is parameterized in RegCM-CLM using the subgrid explicit moisture scheme (SUBEX), which utilizes grid cell averaged relative humidity and cloud fraction to represent subsaturated and saturated fractions within a model grid cell [*Pal et al.*, 2000]. A temperature-dependent autoconversion threshold, Q_c^{th}, is compared to cloud liquid water, Q_c, to determine if precipitation occurs. As temperatures increase, Q_c^{th} increases and affects the precipitation rate (P):

$$Q_c^{\text{th}} = C_{acs} 10^{-0.49+0.013T}, \tag{2}$$

$$P = C_{\text{ppt}}\left(Q_c - Q_c^{\text{th}} FC\right), \tag{3}$$

where T is temperature, FC is fractional cloud cover, C_{acs} is the autoconversion scale factor, and C_{ppt} is an empirically derived autoconversion rate ($C_{\text{ppt}} = 5 \times 10^{-4}$ L s^{-1}). When cloud liquid water (Q_c) exceeds the weighted autoconversion threshold ($Q_c^{\text{th}} FC$), precipitation occurs and falls instantaneously. The difference between cloud liquid water and the weighted autoconversion threshold (ΔQ) physically represents the available precipitable cloud water. Therefore, the formation of large-scale precipitation ultimately depends on temperature, cloud liquid water, and fractional cloud cover. Cumulus precipitation is described by the Grell convection scheme with Arakawa-Schubert closure [*Grell*, 1993], shown to produce the most realistic precipitation in RegCM over North America compared to gridded precipitation products [*Pal et al.*, 2000; *Walker and Diffenbaugh*, 2009].

[10] CLM is the land surface model developed as part of the Community Climate System Model (CCSM), and is described in detail by *Collins et al.* [2006] and *Oleson et al.* [2008]. CLM contains five possible snow layers with an additional representation of trace snow and ten unevenly

spaced soil layers with explicit solutions of temperature, liquid water, and ice water in each layer. Because we extend our analysis to the winter months, soil moisture includes water in both the ice and liquid phase and subsequent discussion refers to "soil moisture" as the sum of soil liquid and soil ice. To account for land surface complexity within a climate model grid cell, CLM uses a tile or "mosaic" approach to capture surface heterogeneity. Each CLM grid cell contains up to four different land cover types (glacier, wetland, lake, and vegetated), where the vegetated fraction is divided into 17 different plant functional types. Hydrological and energy balance equations are solved for each land cover type and aggregated back to the grid cell level. A detailed discussion of CLM version 3 implemented in RegCM3 and a comparative analysis of land surface parameterization options is presented by *Steiner et al.* [2009].

[11] In this version of RegCM-CLM several input files and processes were modified, including the use of high-resolution input data, a soil moisture initialization, and an improved treatment of grid cells along coastlines. For the model input data, CLM requires several time invariant surface input parameters, including soil color, soil texture, percent cover of each land surface type, leaf and stem area indices, maximum saturation fraction, and land fraction [*Lawrence and Chase*, 2007]. The resolution was increased for several input parameters to capture surface heterogeneity when interpolating to the regional climate grid. Soil color, soil texture, glacier, lake, wetland, and land fraction have been improved to 0.05° by 0.05° horizontal spacing, while plant functional types, leaf area index, stem area index, and maximum saturation fraction remain at 0.5° by 0.5° grid spacing. Similar to *Lawrence and Chase* [2007], the number of soil colors was extended from 8 to 20 classes to resolve regional variations. The second modification was to update the soil moisture initialization based on a climatological soil moisture average [*Giorgi and Bates*, 1989] over the use of constant soil moisture content throughout the grid. By using a climatological average for soil moisture, model spin-up time is reduced with regard to deeper soil layers. This is especially true in semiarid conditions, where soil moisture can often take years to equilibrate [*Cosgrove et al.*, 2003]. The third modification to the RegCM-CLM coupling is the inclusion of a mosaic approach for grid cells that contain both land and ocean surface types. With this approach, a weighted average of necessary surface variables was calculated for land-ocean grid cells using the land fraction input data set. This method provides a better representation of coastlines using the high-resolution land fraction data.

2.2. Experiment Design

[12] Model simulations for this study focus on the contiguous United States, with a Lambert conformal projected grid centered at 100°W and 39°N spanning 3625 by 5600 km at 25 km grid spacing. There are 18 vertical atmospheric model layers in sigma coordinates from the surface to 100 mbar. Initial and lateral atmospheric boundary conditions are provided by National Centers for Environmental Prediction (NCEP) reanalysis 1 at 2.5° by 2.5° horizontal spacing and 17 pressure levels (only 8 levels for humidity) every 6 hours [*Kalnay et al.*, 1996]. Weekly updated sea surface temperatures are prescribed using the NOAA Optimum Interpolation SST V2 data set [*Reynolds et al.*, 2002].

[13] Two 23 year simulations from 1982–2004 (inclusive) were performed. The first 2 years are removed in order to allow the model to spin-up and reach equilibrium. The first simulation allows the atmosphere and land surface to interact freely (the interactive run, or RunI) and the land surface model is called every sixth atmospheric model time step, allowing exchange of all variables between the land surface and the atmosphere. The second simulation (the climatological run, or RunC) replaces soil liquid and soil ice with monthly climatological averages from RunI at every land surface time step. Because RunC utilizes prescribed monthly soil moisture, it represents an uncoupled land surface as the lower boundary condition. By comparing the two simulations, we can attribute changes in atmospheric variables to the effects of soil moisture content and phase change. Additionally, if strong land-atmosphere feedbacks are present, we expect to see changes in the mean atmospheric state between the two simulations (further discussion in section 3).

[14] Because prior studies have noted the impact of soil freezing on the climate [*Viterbo et al.*, 1999; *Boone et al.*, 2000; *Niu and Yang*, 2006], soil liquid and soil ice were both held to climatological averages for RunC, capturing the seasonality of soil moisture. Sensitivity of this experiment design is discussed in section 3. As shown in Figure 1 for the North Great Plains (NGP; see box in Figure 3), interannual variability is captured by RunI, while RunC shows a constant seasonal cycle throughout the full simulation because it is forced with constant climatological soil moisture. We focus on the NGP throughout the analysis because of the strong coupling and clear seasonal transition. Other regions were examined and demonstrated a similar coupling mechanism; therefore the NGP is highlighted in subsequent discussion for illustrative purposes of the winter feedback mechanism.

[15] Land-atmosphere coupling strength is evaluated using two methods, the standard deviation difference method, $\Delta\sigma_T$ [*Seneviratne et al.*, 2006; *Zhang et al.*, 2008a] and the GLACE coupling parameter, $\Delta\Omega$ [*Koster et al.*, 2006]. The standard deviation method is defined as:

$$\Delta\sigma_T = \sigma_{\mathrm{RunI}} - \sigma_{\mathrm{RunC}} \tag{4}$$

where σ_{RunI} and σ_{RunC} are the standard deviations of 2 m air temperature for RunI and RunC, respectively. Because the only difference between the RunI and RunC simulations is the treatment of soil moisture, the difference between the standard deviations of RunI and RunC should describe the degree to which surface air temperature variations are caused by changes in soil moisture magnitude and soil moisture phase.

[16] The GLACE coupling parameter has generally been used during the summer by dividing the June–August (JJA) period into 16 pentads (neglecting the first 10 days of the summer) for a specific atmospheric variable [*Koster et al.*, 2004; *Koster et al.*, 2006; *Seneviratne et al.*, 2006; *Zhang et al.*, 2008a]. Here we focus on the spring transition months (March–May) when employing $\Delta\Omega$, neglecting the first 12 days to maintain a 16 pentad season. Parameter $\Delta\Omega$ is defined as Ω_X(RunI) − Ω_X(RunC) where Ω_X is

$$\Omega_X = \left(N\sigma^2_{\langle X\rangle} - \sigma^2_X\right) \Big/ \left((N-1)\sigma^2_X\right), \tag{5}$$

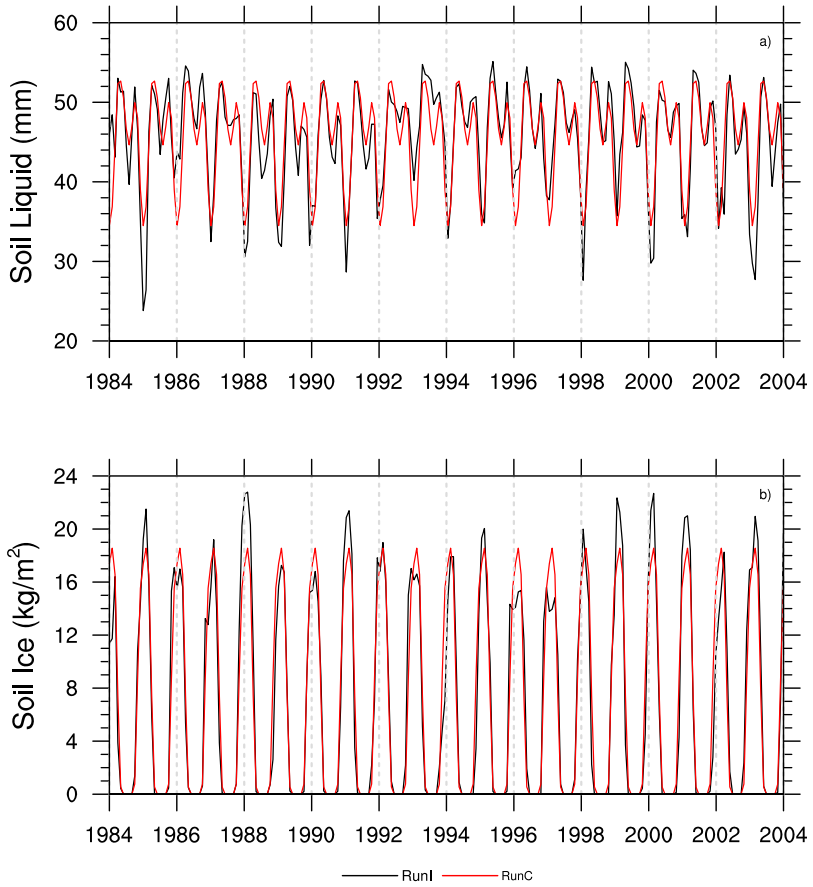

Figure 1. Interannual variability of the surface soil layer (top 10 cm) of (a) soil liquid (mm H_2O) and (b) soil ice (kg m^{-2}) for RunI (black) and RunC (red) over the Northern Great Plains region (NGP; see box in Figure 3).

N is the number of simulation years (=21), $\sigma^2_{\langle X \rangle}$ is the variance across average pentads, and σ^2_X is the variance of every pentad for all years (e.g., 21 years by 16 pentads).

[17] *Zhang et al.* [2008a] demonstrated that the standard deviation differencing method yields similar results over the contiguous United States to the coupling strength parameter [*Koster et al.*, 2006] and the variance method [*Seneviratne et al.*, 2006]. For this analysis, $\Delta\sigma_T$ is used to identify regions where coupling between the land surface and air temperatures exists (sections 4.2–4.4), whereas $\Delta\Omega$ is used to described similarity of liquid precipitation between pentads for March through May (section 4.5.3).

[18] Our assessment of the coupling strength is similar to GLACE with several notable exceptions: (1) a single model is used for multiple years, unlike GLACE which performed ensemble simulations with 12 different AGCMs for one season; (2) the model simulations are at a higher spatial resolution of 25 km; (3) simulations are continuous (e.g., simulations are run continuously for 23 years, while GLACE performed 16 member ensembles per model for only JJA); and (4) analysis is extended to all seasons.

3. Coupling Strength Sensitivity

[19] In order to assess the sensitivity of coupling strength to the treatment of soil ice, two additional 7 year simulations were performed from 1982–1988 with the first two years discarded for model spin-up. Similar to RunC, one simulation prescribes 50% of the climatological soil ice and 100% of the soil liquid water from RunC (run ICE50). By comparing RunC and ICE50 simulations to the RunI simulation, we can assess the influence of the amount of soil ice on coupling strength and interannual variability. The second simulation holds the total soil water mass (liquid + ice) constant and allows ground temperatures to determine the phase of water in the soil (MASS). The MASS simulation helps identify regions where interannual variability of total soil moisture (liquid + ice) has the greatest impact on the atmosphere.

[20] The standard deviation coupling strength method for 2 m air temperature is calculated for each of the three climatological simulations (RunC, ICE50, and MASS) relative to RunI (e.g., $\Delta\sigma_T^{\text{climatological}} = \sigma_{\text{RunI}} - \sigma_{\text{climatological}}$; Figure 2). When comparing the $\Delta\sigma_T$ values across the three sensitivity tests, the spatial distribution of coupling strength is similar for RunC and ICE50. Notably, RunC and ICE50 have similar coupling strength magnitudes in March and April over the central and northern Plains (>0.8 K), suggesting the magnitude of ice prescribed does not have a strong influence on the magnitude of land-atmosphere coupling parameter.

[21] The coupling strength is markedly weaker in the MASS simulation than in the other two climatological simulations with fixed amounts of soil ice (RunC and ICE50). Further, MASS demonstrates no distinct spatial coupling

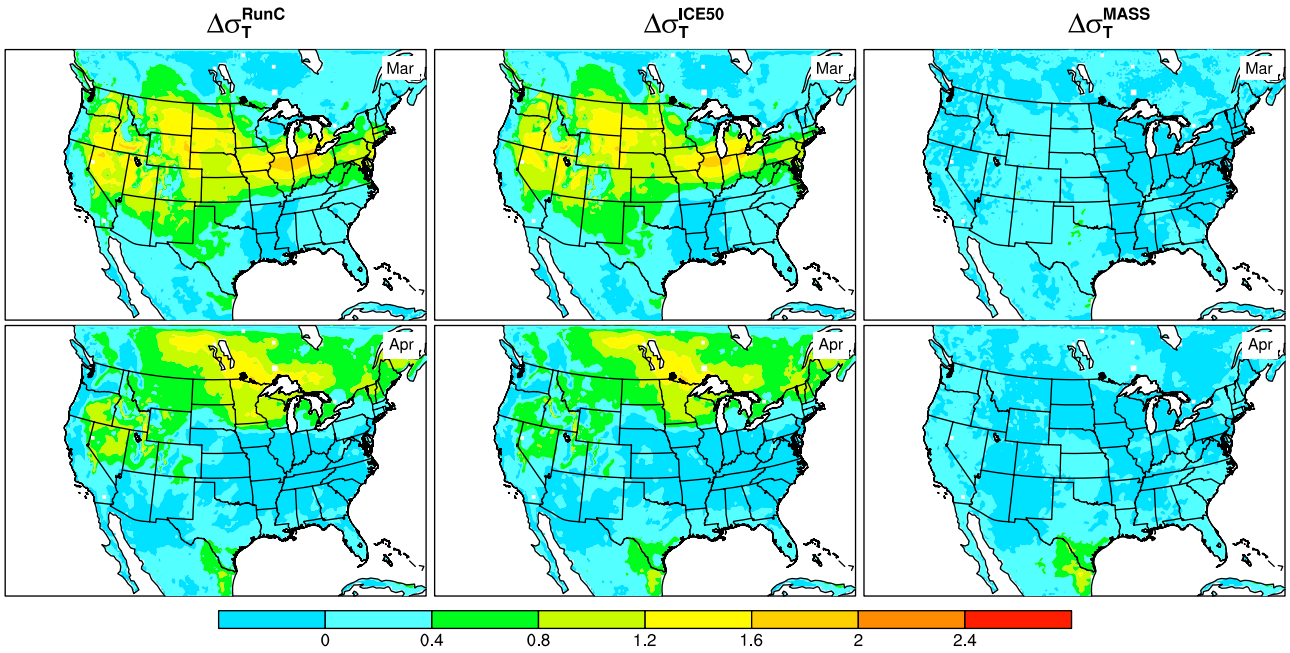

Figure 2. March and April coupling strengths, $\Delta\sigma_T = \sigma_{\mathrm{RunI}} - \sigma_{\mathrm{climatological}}$, for three simulations where warmer colors signify stronger land-atmosphere coupling.

pattern with weak to no coupling over much of the United States (<0.4 K), indicating that the interannual variability of 2 m air temperature is similar for MASS and RunI. Unlike traditional land-atmosphere coupling studies performed for summer, soil water phase transitions provide additional complexity. By introducing phase change in MASS, soil moisture is no longer constant interannually for soil liquid and ice individually. Soil water freezing (melting) can then be regarded as an energy and moisture sink (source). As a consequence, soil liquid water available for evaporation changes from year to year, dampening the response in the land-atmosphere coupling parameter. Because the goal of our study is to evaluate the role of soil water phase on land-atmosphere coupling, the interannual variability of soil liquid/ice partitioning in MASS complicates the assessment of the role of soil water phase on land-atmosphere coupling. Therefore, subsequent discussion regarding the feedback mechanism compares RunI and RunC to highlight the role of soil moisture phase in land-atmosphere coupling.

[22] Although by design there is no interannual variability in soil liquid and ice for the climatological simulations (RunC and ICE50), the climatological method has specific behaviors that merit discussion. Because soil ice is prescribed in these simulations, the atmosphere could continue to transfer energy into the soil column attempting to melt a persistent soil ice mass during conditions when the atmosphere is warmer than the land surface. When soil ice is present, energy that would have warmed the land surface is now transferred into the ground to melt the soil ice. Therefore in the climatological simulations, the mean climate may become colder than RunI. However, this cold bias does not affect the magnitude or spatial pattern of coupling because the standard deviation method, equation (4), effectively removes mean bias and represents interannual variability about the mean condition. As noted above, the magnitude of ice did not have a strong effect on the coupling strength (RunC and ICE50 have similar coupling strengths; Figure 2), suggesting that the presence of ice phase is key to the land-atmosphere coupling.

4. Results

4.1. Model Evaluation of Climate Variables

[23] To evaluate the ability of RegCM-CLM to reproduce the mean climate state, we compare modeled temperature and precipitation results against the monthly 0.5° gridded observational data set developed by the Climate Research Unit (CRU) at East Anglia [*Mitchell and Jones*, 2005]. Because CRU data are only available through the end of 2002, we compare the model versus measurements for the time period 1984–2002. The RegCM-CLM produces a warm bias over the Great Plains that is prevalent during each season (Figure 3). During March–May (MAM) and September–November (SON), the model is on average 1–2 K warmer from northern Texas through central Canada, with some localized biases exceeding 3 K. Summertime (June–August, JJA) has a warm bias of similar magnitude, but the bias extends further east over the Great Lakes region. Winter (December–February, DJF) demonstrates the largest deviation from observed temperatures in the NGP and Canada (1–4 K warmer than CRU), a feature common to most regional climate models [*Walker and Diffenbaugh*, 2009]. In addition to the warm bias over the Great Plains, there is a consistent 1–3 K cool bias over western Mexico. Despite these biases in surface temperature, the model reproduces the seasonal cycle of temperatures on a regional basis in the South, Northeast, and our NGP analysis region. The modeled interannual variability of temperature can also be compared to the observed temperature interannual variability through the relative model bias of interannual variability (defined as $1 - \sigma_{\mathrm{RunI}}/\sigma_{\mathrm{OBS}}$; Figure 3). For temperature, the model shows less interannual variability over much of the central United

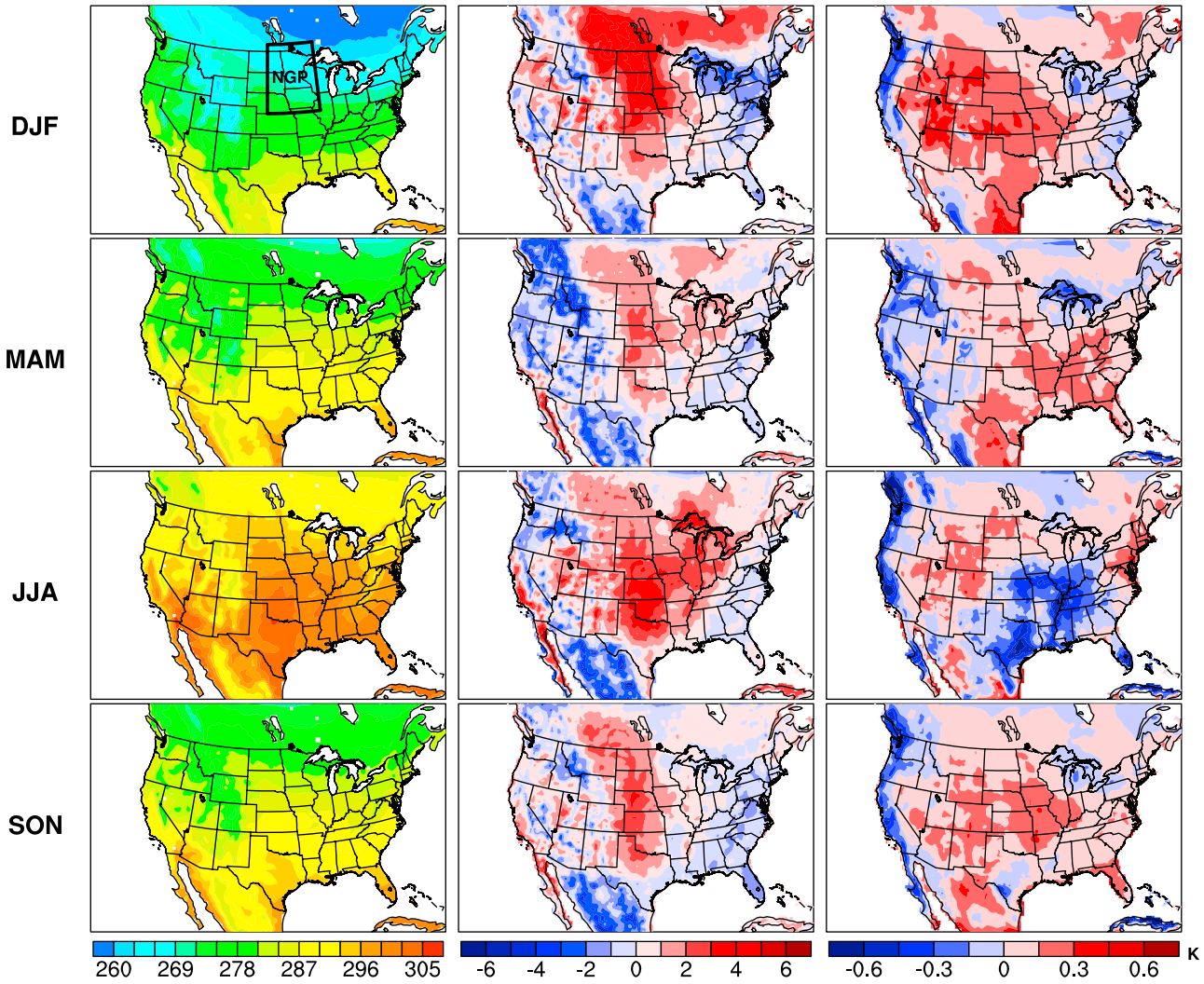

Figure 3. (left) Seasonal temperatures (K), (middle) absolute biases compared to CRU, and (right) relative bias of interannual variability ($1 - \sigma_{\mathrm{Runl}}/\sigma_{\mathrm{CRU}}$). Red (blue) colors imply the model is warmer (colder) than CRU observations for absolute bias (Figure 3, middle). For relative bias of interannual variability (Figure 3, right), red (blue) colors imply the model has less (more) interannual variability than CRU observations. The black box identifies the Northern Great Plains (NGP; 40°N–50°N and 100°W–90°W) averaging region used in subsequent analysis.

States and Mountain West regions for winter, spring, and fall. During summer in the Southeast, the model has more interannual temperature variability than observed, suggesting that land-atmosphere coupling may be overestimated by the model in these regions in the summer (Figure 3).

[24] Precipitation in RegCM-CLM tends to be greater than observed in the western United States throughout the year. Areas with complex topography yield the greatest discrepancies between modeled and observed precipitation. Specifically, western Mexico and the Pacific Northwest show the greatest wet bias in the model throughout the year (>60 mm per month; Figure 4), correlated with locations that have the greatest annual precipitation amounts. This overestimation of precipitation over complex terrain is common to many regional climate models [*Leung et al.*, 2003; *Duffy et al.*, 2006; *Wang et al.*, 2009]. The northern Plains are wetter by 10–35 mm per month than observed for DJF and MAM, with improved agreement in SON. The southeastern United States tends to be drier than observed (20–50 mm per month) for SON and DJF and wetter during JJA (15–35 mm per month), with maxima along the eastern seaboard north of the 35th parallel. The model shows similar difficulty capturing interannual variability over complex terrain, generally overestimating interannual precipitation variability over much of the U.S. domain. However, the best performance in capturing interannual variability occurs during the fall and spring east of the Rocky Mountains (Figure 4). A discussion of the coupling strength results will be described with respect to these model biases (section 6).

4.2. Seasonal Evolution of Coupling Strength

[25] Based on $\Delta\sigma_T$ definition of coupling strength, equation (4), we note a strong coupling region over the southern and central Great Plains during the warmer months (June–September) (Figure 5). More specifically, temperatures vary 0.5–1 K more with interactive soil moisture

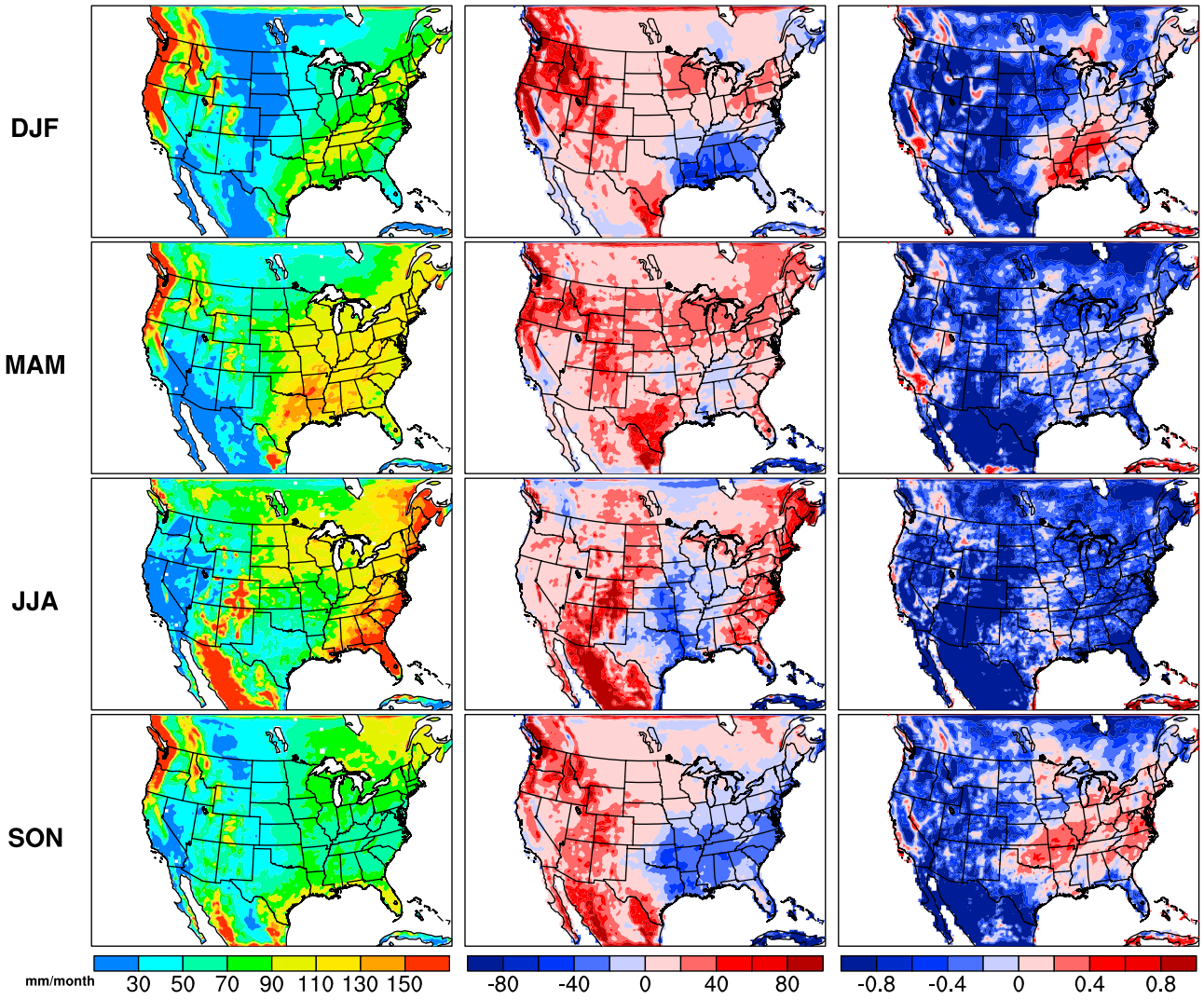

Figure 4. (left) Seasonal precipitation (mm per month), (middle) absolute biases compared to CRU, and (right) relative bias of interannual variability ($1 - \sigma_{RunI}/\sigma_{CRU}$). In Figure 4 (middle), redder (blue) colors imply the model is wetter (drier) than CRU observations. In Figure 4 (right), redder (bluer) colors imply the model has less (more) interannual variability than CRU observations.

(RunI) for May–September over Texas and Oklahoma. While there is general agreement regarding the southern Plains hotspot found by GLACE [*Koster et al.*, 2004; *Koster et al.*, 2006], the strong coupling region extends eastward into the Tennessee and Ohio River Valleys in August indicating a broader spatial coverage than prior studies (results not shown).

[26] When extending our analysis to the colder months (October–April), we find a more pronounced coupling strength compared to summer. The magnitude of temperature variability attributable to variations in soil moisture content and phase increases during the fall to winter transition. The soil-moisture driven variability peaks in February at 0.75–1.5 K, then gradually decreases in strength in the spring (March–May) (Figure 5). In addition to having stronger coupling, the coupled region covers a broader spatial extent, present from the foothills of the Rocky Mountains eastward to the Atlantic coast (Figure 2). The broad winter coupling pattern first appears in October, primarily over central Canada (Figure 5). The region then migrates toward the southeastern United States by January and northward once again into Canada during spring, eventually disappearing by June. This migration of coupling strength appears to follow the freezing line as it migrates with season. In sections 4.3–4.5, we examine the cold regime land-atmosphere feedback mechanism that produces this pattern and summarize the winter land-atmosphere feedback mechanism in section 5.

4.3. Coupling Strength Relation to Soil Liquid Water and Surface Energy

[27] Surface energy fluxes are a primary mechanism of energy transfer between the land surface and the atmosphere. Here, we define the available surface energy as the sum of sensible and latent heat from the surface and the available surface energy deficit as difference in available surface energy between RunI and RunC. During the transition months over the NGP region, latent and sensible heat

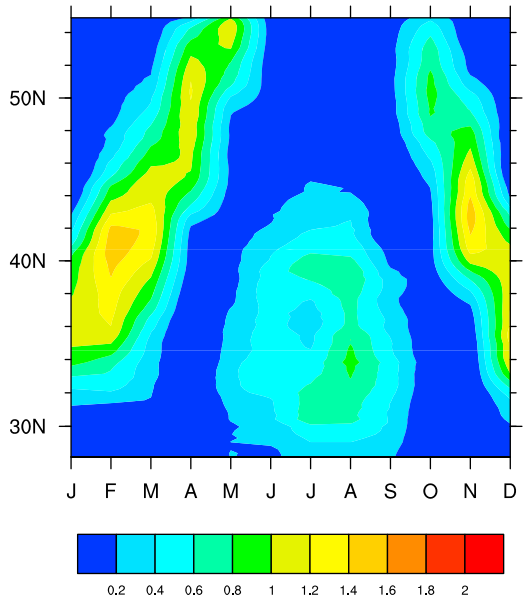

Figure 5. Seasonal meridional coupling strength, $\Delta\sigma_T = \sigma_{\mathrm{RunI}} - \sigma_{\mathrm{RunC}}$, averaged over 100°W–90°W.

contribute approximately the same amount to available surface energy (e.g., the Bowen ratio is not substantially different between the two runs; figure not shown). The sign of available surface energy flux varies with both time and space. Positive values indicate that the land surface is a source of energy to the atmosphere, while negative values suggest that the ground temperatures are cooler than the overlaying atmosphere thereby drawing down heat from the atmosphere and acting as a heat sink.

[28] We focus on March to isolate the winter-to-spring transition of the coupling strength, and evaluate a meridional cross section from 23°N to 55°N (averaged from 100°W to 90°W) of available surface energy, coupling strength, ground temperature, and net surface longwave radiation interannually and climatologically (Figure 6). In March, available surface energy differences between RunI and RunC occur around the 40th parallel with differences of 30–75 W m^{-2} (Figure 6a). Additionally, Figure 6d illustrates that areas with increased available surface energy are colocated with more intense coupling. Along the transect, RunI has approximately 30 W m^{-2} more available surface energy than RunC for December and January and approximately 50 W m^{-2} for February–April.

[29] Because available surface energy and ground temperature are strongly correlated, the ground temperature is a key component of the land-atmosphere feedback mechanism. In the coupled region, RunC is 1–7 K colder than RunI (Figures 6b and 6e). In March, the surface soil temperature is often below the freezing point at latitudes 4°–8° farther south in RunC compared to RunI (Figure 6b). This indicates that climatological soil moisture simulations are colder throughout the simulation period, leading to less available surface energy in RunC. Additionally, the coupling strength tends to peak slightly south of the freezing line in RunI. Once both simulations have reached the freezing line, the available surface energy deficit and ground temperatures are nearly identical with increasing latitude. The sharp changes in the north-south temperature gradient in RunC indicate that temperatures reach freezing more rapidly than in the fully interactive run (RunI). For 1996 and 2002, the coldest March years, the freezing line in RunI approaches the RunC freezing line, corresponding to weaker temperature differences.

[30] As ground temperatures change, we could also expect a change in the surface snow cover. A common land-atmosphere feedback in cold climates is the temperature–snow albedo feedback, where colder temperatures lead to the presence of more snow on the ground, increasing the albedo and reducing absorbed solar radiation, thereby enhancing the colder temperatures [*Yang et al.*, 2001; *Bony et al.*, 2006]. We evaluate this feedback in our two simulations, and find that absorbed solar radiation at the surface is not substantially different between RunI and RunC (<5% difference; figure not shown). This indicates that albedo modifications induced by variable snow or cloud cover are likely not the driver for the observed differences in available surface energy and ground temperature between the two simulations. However, there are noticeable changes in net surface longwave radiation (Figures 6c and 6f). Longwave radiation shows similar behavior to ground temperature and available surface radiation, with maximum differences in March occurring around 40°N, and migrating seasonal behavior. Further, March years with the greatest longwave radiation differences (1986 and 1991) correspond to years containing the greatest ground temperature differences. This implies much of the difference in longwave energy is likely due to warmer ground temperatures in RunI.

[31] In March, the interannual variability of ground temperature differences between RunI and RunC follow the differences in surface percent soil liquid water (Figure 7; surface soil layer defined as ~10 cm depth). This relationship is particularly clear during March 2002 where there is a large difference in percent soil liquid (RunI 14% less percent soil liquid as water) and a corresponding decrease in ground temperature differences (RunI colder by 0.5 K). This indicates that the percent of soil moisture in the liquid phase is important in controlling ground temperature variability over coupled regions.

4.4. Soil Temperature and Moist Static Energy

[32] As described above, the percentage of soil moisture that is liquid water appears to be a driving variable that affects ground temperature and the amount of surface energy that can propagate into the atmosphere. The soil column temperature can act as a slowly varying heat reservoir and explain changes in the available surface energy on a seasonal scale. Figure 8 displays the difference (RunI minus RunC) in soil temperature and moist static energy (MSE) atmospheric profiles for the same meridional cross section and time period as Figure 6. Throughout the column, the soil temperature for RunI is 2–5 K warmer than RunC during March (similar to surface ground temperature). Additionally, the peak soil temperature differences occur between 0–20 cm (Figure 8a). From January–May, there is a clear northward migration of the soil temperature maximum (Figure 8b). By May, the temperature differences have weakened, implying conduction by the soil column toward the surface and a release of this energy to the atmosphere in RunI. Again, we note that the deviation in RunC soil

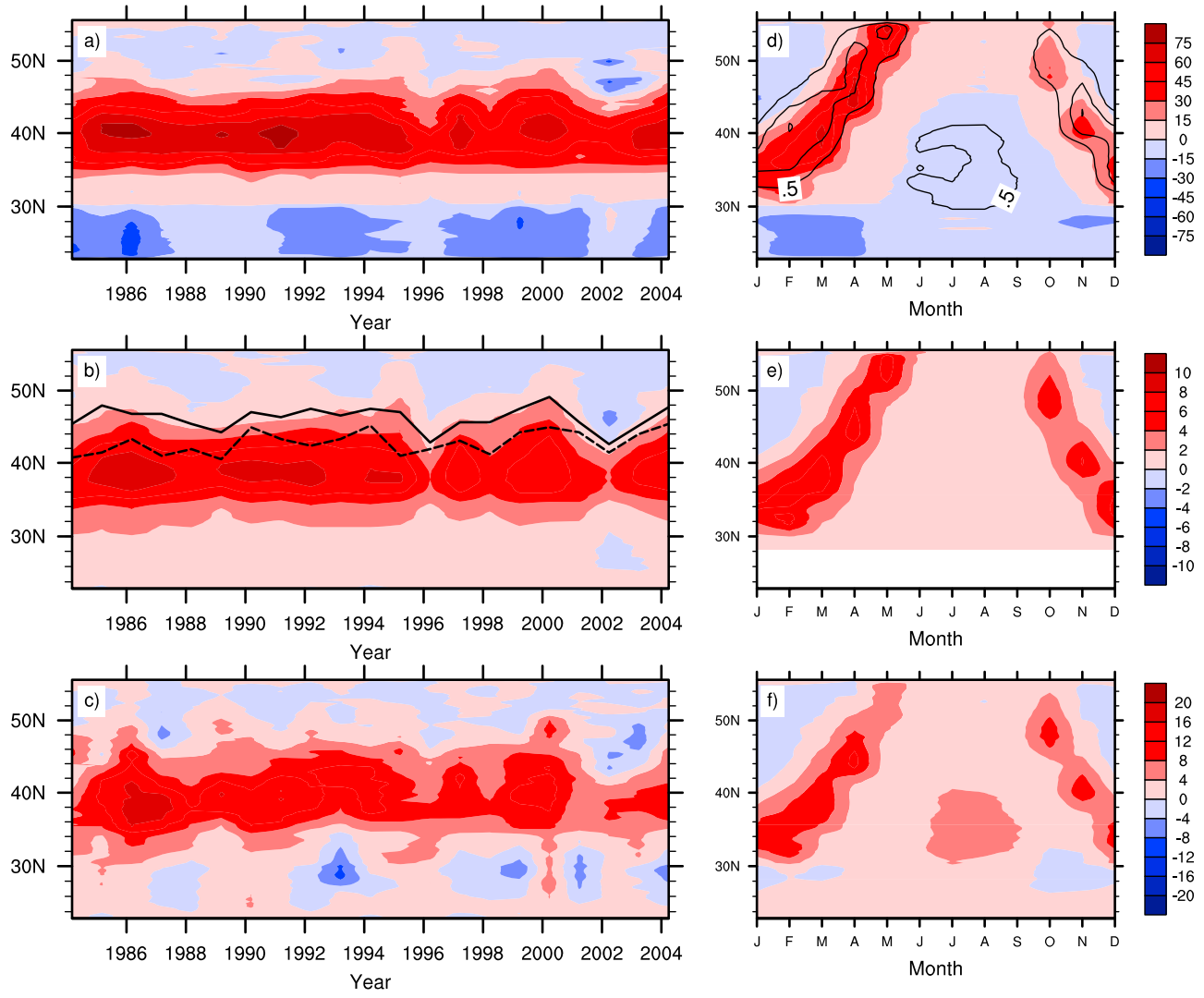

Figure 6. Meridional averages (100°W–90°W) of March interannual variability for differences between RunI and RunC (RunI-RunC) for (a) available surface energy (W m^{-2}), (b) ground temperature (K), and (c) surface net longwave radiation (W m^{-2}) and meridional (100°W–90°W) climatological averages of (d) available surface energy, (e) ground temperature, and (f) surface net longwave radiation (W m^{-2}). Solid and dashed lines in Figure 6b represents RunI and RunC freezing lines, respectively. Contours in Figure 6d represent coupling strength ($\Delta\sigma_T$).

temperatures from the climatological mean is due to the persistent presence of ice. While this likely overestimates the persistence of ice compared to true conditions, it highlights the role of soil ice in land-atmosphere coupling.

[33] Moist static energy is defined by

$$\mathrm{MSE} = c_p T + L_v q + gz, \tag{6}$$

where c_p is specific heat capacity at constant pressure, T is temperature, L_v is the latent heat of vaporization, q is water vapor mixing ratio, g is acceleration from gravity, and z is height. MSE is used as an indicator of instability within the troposphere [*Emanuel*, 1995; *Pal and Eltahir*, 2001]. In March, the MSE profile model differences are tightly colocated with the soil temperature differences. MSE for RunI is 1–8 kJ kg^{-1} greater, with changes reaching as high as 700 mbar (Figure 8a). This suggests that the soil temperature changes have the ability to affect the vertical profile of MSE, thereby creating a land-atmosphere feedback during the months in the transition from winter to spring.

4.5. Effects on Precipitation

[34] During the colder months (October–April) in the northern midlatitudes, precipitation typically occurs as a result of large-scale frontal features rather than local convective precipitation. Our simulations show a distinct soil moisture–precipitation feedback occurring during these winter months, and we evaluate contributions from convective and large-scale precipitation as well as the phase of precipitation. In the NGP, the greatest precipitation changes occur in the transition seasons, with total precipitation in RunI increasing 21% in April and 22% in November compared to RunC (Figures 9a and 9b). When examining the relative contributions of large-scale and convective

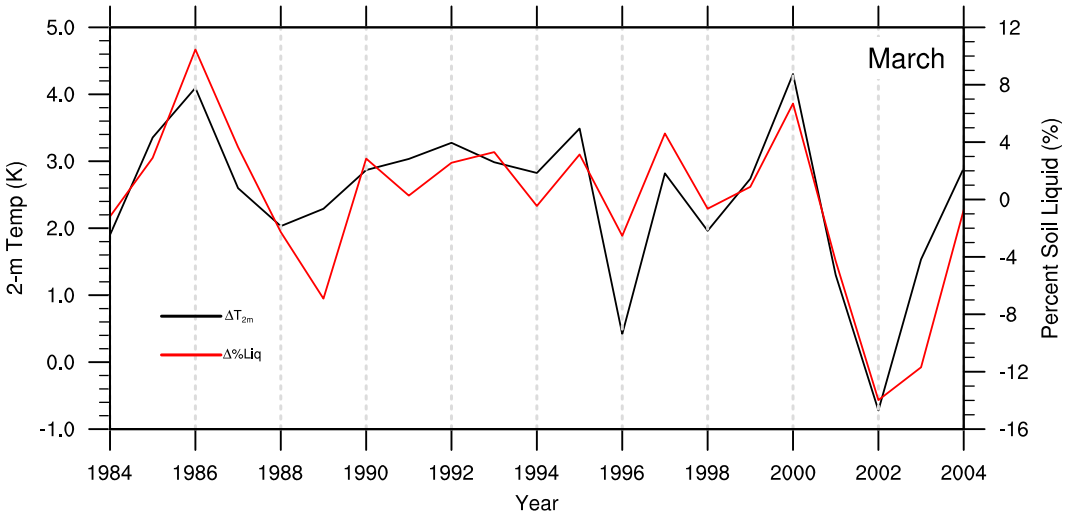

Figure 7. Interannual variability of the difference of ground temperature (RunI − Run C; black) and the difference in percent soil water as liquid (RunI − RunC; red) during March averaged over the NGP region.

precipitation to the total winter precipitation, two distinct signatures arise: 1., Changes in convective precipitation and large-scale precipitation contribute roughly equally to the increase in total precipitation (April and October, Figure 9b); and 2., large-scale precipitation contributes >80% to the increase in total precipitation (November and March, Figure 9b). Section 4.5.1 focuses on the first signature and the mechanism controlling the increase in convective

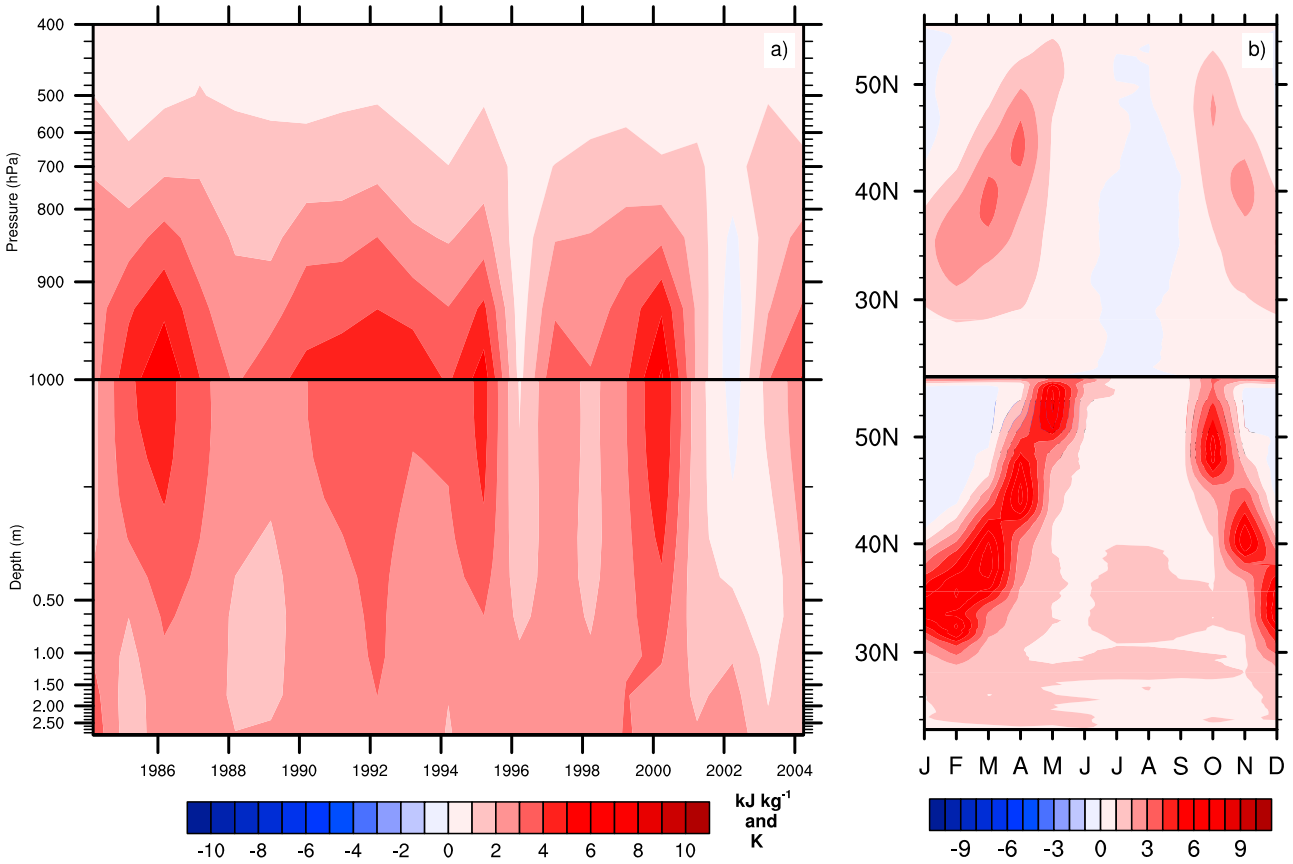

Figure 8. Meridional averages (100°W–90°W) of (a) March interannual variability and (b) annual climatologically averaged differences between RunI and RunC (RunI − RunC) for vertical profiles of moist static energy (MSE, kJ kg^{-1}; top) and soil temperature (K; bottom). Red (blue) colors mean RunI is warmer (colder) or has more (less) MSE than RunC.

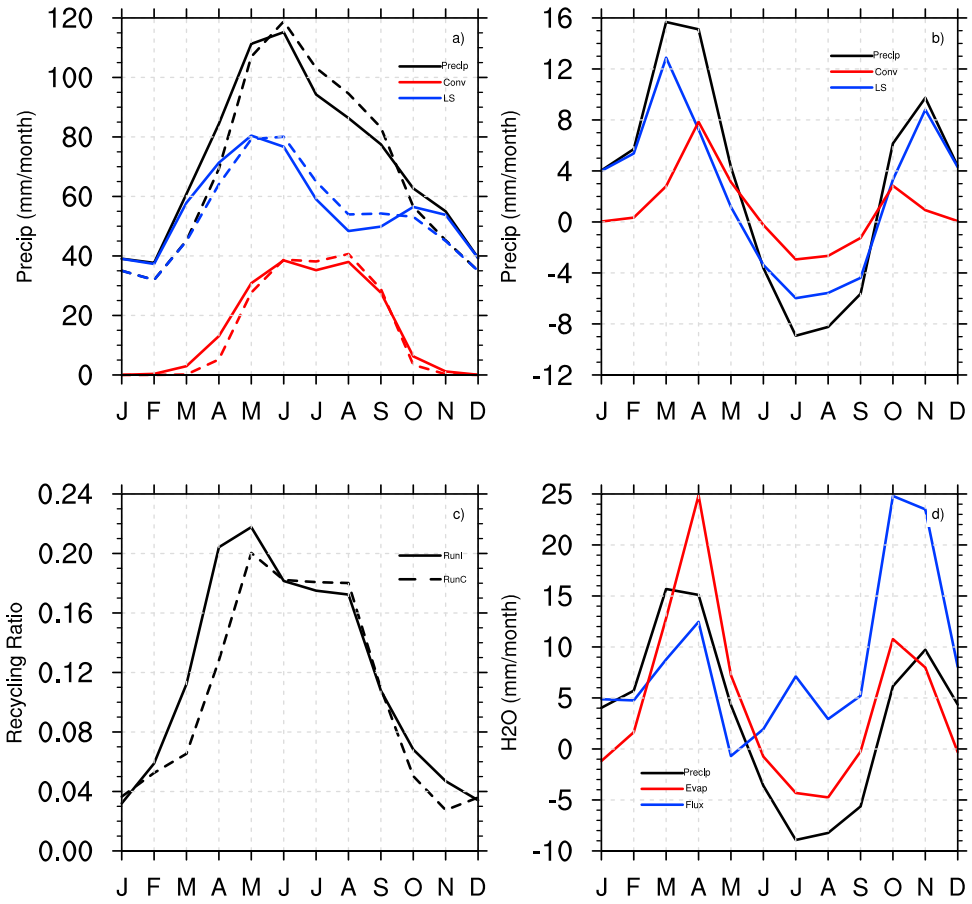

Figure 9. (a) Monthly climatologies of large-scale, convective, and total precipitation for RunI (solid) and RunC (dashed). (b) Monthly climatological differences (RunI − RunC) for contributions of large-scale (blue) and convective (red) precipitation to the total (black). (c) Monthly climatologies of recycling ratio (β) for RunI (solid) and RunC (dashed). (d) The difference (RunI − RunC) in atmospheric moisture sources for total precipitation (black), moisture flux into the region (blue; *IN* from equation (1)), and evapotranspiration within the region (red; *ET* from equation (1)). All are averaged over the NGP region shown in Figure 3.

precipitation, while the second signature dominated by large-scale precipitation is discussed in section 4.5.2. The phase of precipitation is analyzed and discussed in section 4.5.3.

4.5.1. Convective Precipitation

[35] The recycling ratio (β, equation (1)) is an indicator of local moisture recycling efficiency, and the degree of local moisture influence is illustrated in the monthly climatology of β over NGP (Figure 9c). The peak difference in recycling between simulations occurs in April (RunI is greater by 0.07) and to lesser extent in October (RunI is greater by 0.02). In April, evaporation is greater for RunI by 25 mm per month, which is about two times the magnitude of change in moisture flux into the region (Figure 9d). During peak evaporation (April and October) we find a corresponding increase in convective precipitation, implying a local feedback between evaporation and convective precipitation consistent with a higher β.

[36] The convective precipitation mechanism is linked to the amount of evaporated surface moisture in the region. Specifically, surface evaporation is incorporated into the available surface energy calculation as latent heat flux; therefore increases in evaporation are reflected as increases in available surface energy. As ground temperature increases (Figure 6b), available surface energy also increases (Figure 6a) providing additional energy flux into the atmosphere. This energy transfer from the surface to the atmosphere translates into elevated MSE (Figure 8a) that in turn promotes convective precipitation. Because differences in these surface and atmospheric variables have nearly identical seasonal cycles, this strongly suggests the presence of a positive land-atmosphere feedback cycle. This type of feedback cycle is the one that drives the summertime feedbacks of most land-atmosphere coupling studies [e.g., *Koster et al.*, 2004], yet we note its presence in a relatively colder region and also outside of boreal summer.

4.5.2. Large-Scale Precipitation

[37] Although convective precipitation contributes to roughly half of the precipitation increases seen in October and April (Figure 9b), large-scale precipitation dominates the change in precipitation in the colder transition months (November and March). The ΔQ_{Tot} profile (Figure 10a) describes the difference in large-scale precipitation occurring at each level in the atmosphere, as precipitation is merely ΔQ multiplied by the autoconversion rate, C_{ppt} (equation (3)). The March–

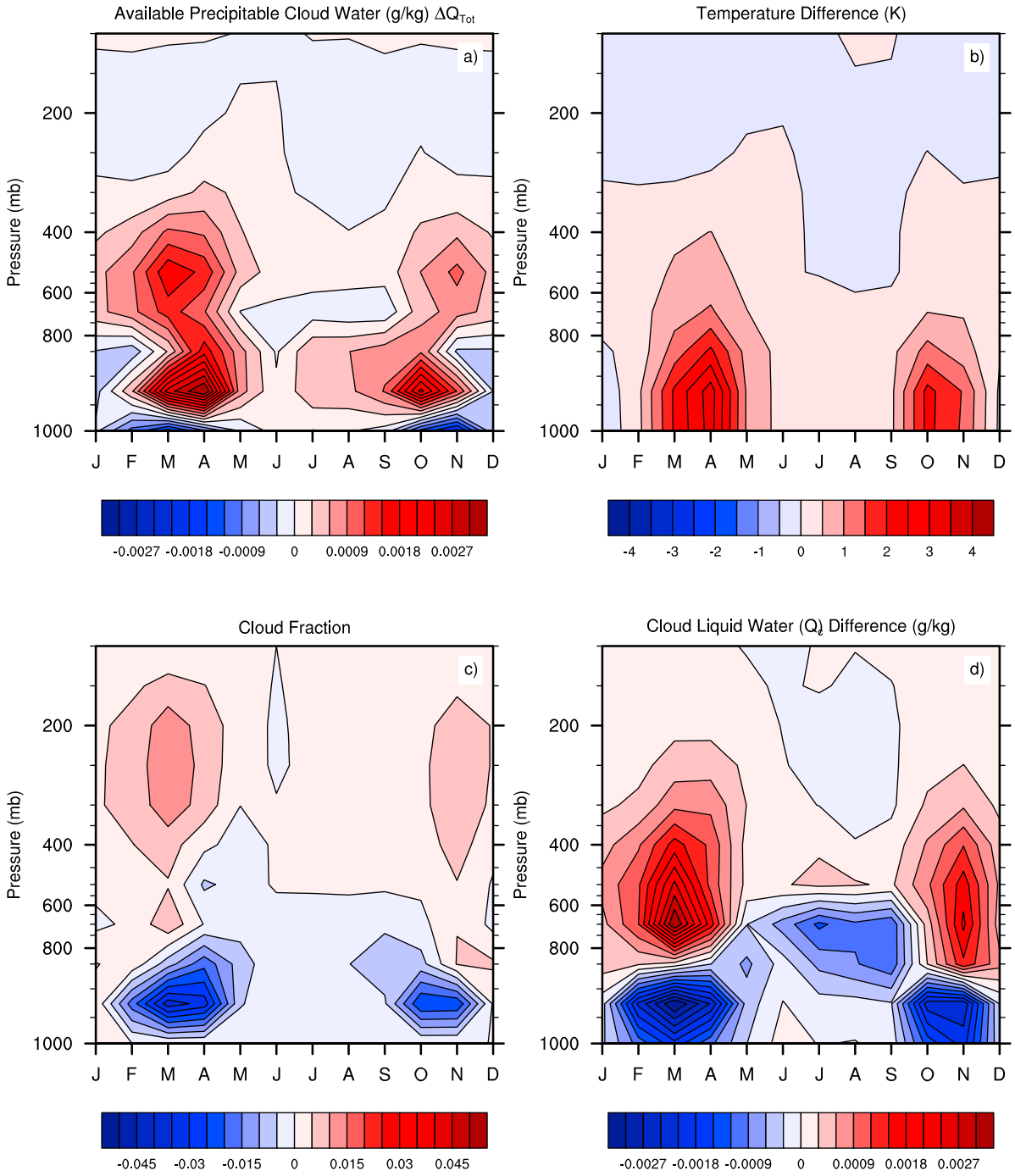

Figure 10. Monthly climatological difference between RunI and RunC over the NGP for (a) available precipitable cloud liquid water (ΔQ_{tot}), (b) temperature (K), (c) cloud fraction, and (d) cloud liquid water. Warmer (cooler) colors indicate that RunI (RunC) values are greater than RunC (RunI).

April and October–November time periods have a greater amount of large-scale precipitation in RunI. Further, there are two clear levels in the atmosphere where large-scale precipitation is noticeably elevated, at 500 mbar and 950 mbar. The atmospheric temperature profile (Figure 10b) indicates that RunI is warmer by 2–3.5 K during the coupled months and the warm anomaly extends to approximately 700 mbar. The temperature profile also indicates that there is less warming occurring in March and November relative to April and October, months when convection contributes more to total precipitation. Warmer temperatures increase the autoconversion threshold and inhibit large-scale precipitation. However, we find there is an increase in large-scale precipitation below 700 mbar coincident with increasing temperatures for RunI. Large-scale precipitation differences below 700 mbar can only then be attributed to reduced fractional cloud cover (Figure 10c) in RunI through decreasing the weighted autoconversion threshold ($Q_c^{th}FC$). As $Q_c^{th}FC$ increases (decreases), it takes more (less) cloud liquid water to reach saturation and produce precipitation.

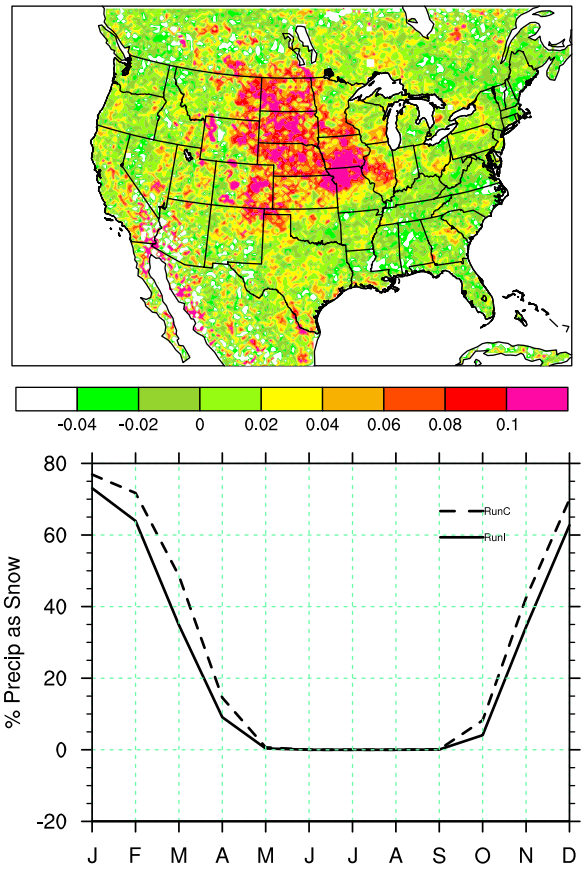

Figure 11. (top) GLACE coupling parameter, $\Delta\Omega$, of liquid precipitation for MAM and (bottom) monthly mean climatology of percent precipitation as snow for RunI (solid) and RunC (dashed).

Therefore, less low-level cloudiness in RunI allows for more large-scale precipitation by lowering the autconversion threshold.

[38] Since temperature differences are primarily restricted to below 700 mbar, temperature differences cannot account for the changes in large-scale precipitation seen at 500 mbar. Figure 10d shows the vertical profile of cloud liquid water differences between the two simulations where warmer (cooler) colors imply more cloud liquid water for RunI (RunC). March and November have the greatest increases in cloud liquid water above 700 mbar. The increase in cloud liquid water and relatively similar values of temperature and cloud fraction between simulations demonstrate that elevated cloud liquid water causes the increase in large-scale precipitation higher in the atmosphere.

[39] To summarize, large scale precipitation–soil moisture feedback is dictated by two factors. The first factor is greater low-level (<700 mbar) cloud fraction in RunC increases the autoconversion threshold, thereby inhibiting large-scale precipitation. Since cloud fraction is calculated using relative humidity [*Pal et al.*, 2000], the colder air temperatures in RunC tend to produce higher cloud fraction with less available moisture. This results in persistent nonprecipitating clouds for RunC (Figures 10a and 10c). The second factor is greater cloud liquid water at higher levels in the atmosphere (>700 mbar). With greater cloud liquid water, RunI is likely to exceed the autoconversion threshold and produce precipitation. The two factors are not independent in that with greater low-level cloud cover, evaporated surface moisture is less likely to extend higher into the atmosphere. To that effect there is less moisture aloft (>700 mbar) in RunC and less large-scale precipitation throughout the column.

4.5.3. Precipitation Phase

[40] In addition to differences in total precipitation (convective and large scale), the phase of precipitation also differs in the NGP region. During the winter and transition months RunC has 3–14% more total precipitation falling as snow (Figure 11b). The maximum differences in percent precipitation as snow coincide with the greatest differences in total precipitation (Figure 9b). This implies that RunI not only has more total precipitation during the transition months, but also a greater percent of precipitation falling in the liquid phase. While this change in phase does not make a substantial difference in the amount of snow cover on the ground, it does appear to influence amount of liquid water in the soil. Using the GLACE coupling parameter to examine liquid precipitation similarity across pentads for March through May, we find a clear region of soil moisture–liquid precipitation coupling over the northern and central Great Plains (Figure 11a). This indicates that liquid precipitation falling in one pentad coincides with subsequent liquid precipitation in other pentads over the coupled region. This identifies the northern and central Great Plains as regions with an intraseasonal soil moisture–precipitation feedback during the March transition season.

5. Discussion of Winter Feedback Mechanism

[41] The feedback diagram presented in Figure 12 broadly describes the proposed winter feedback mechanism with associated correlation coefficients between variables involved in the convective precipitation feedback for NGP (April and October). Correlations for the large-scale precipitation portion of the feedback were not included due to the complex processes occurring at multiple layers in the atmosphere to produce large-scale precipitation. During colder months, our results indicate that the soil water phase plays a role in moderating soil temperatures as shown by strong correlation between percent soil moisture as liquid and subsurface temperatures (correlation coefficient (r) = 0.626; Figure 12). For years with warmer winters, the amount of available surface energy increases (r = 0.397 for ground temperature and available surface energy), leading to an increase in liquid phase precipitation (Figures 9 and 11). This causes more water to enter the soil column resulting in warmer surface temperatures during the cold season in RunI. This tendency of precipitation–soil moisture feedbacks to moderate especially cold temperatures in RunI prevents ground and air temperatures from reaching the freezing point during the transition into and out of winter (Figure 6). As such, subsequent precipitation events are more likely to produce liquid phase precipitation (Figure 11) that can further contribute to the feedback cycle. In contrast, RunC has a fixed amount of soil liquid water and ice, resulting in colder climatological temperatures due to the lack of land-atmosphere feedbacks and persistent soil ice. While this feedback is likely amplified by the persistent soil ice in the experiment

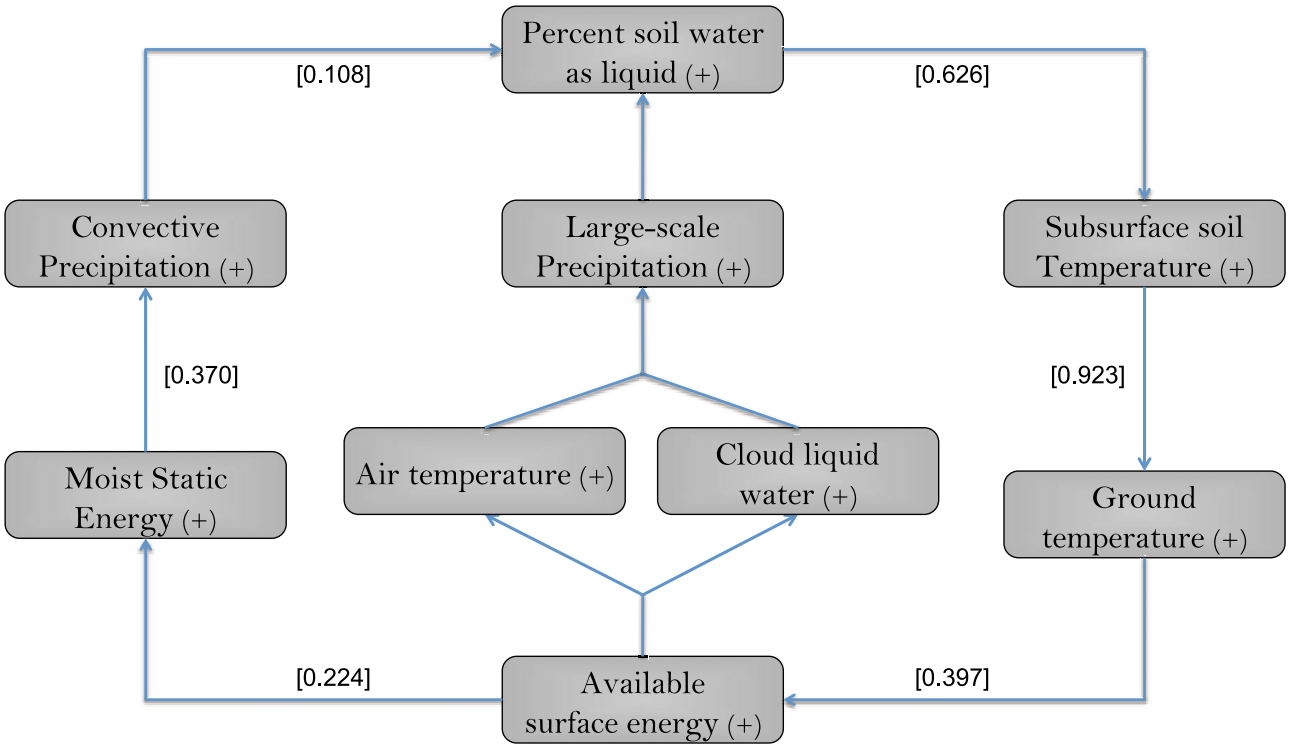

Figure 12. Winter land-atmosphere feedback mechanism with cross-variable correlations for $\Delta\sigma_T > 1$ K east of Rocky Mountains during April for RunI.

construct, it highlights the role of soil ice in cold season land-atmosphere coupling.

[42] The land-atmosphere feedbacks can affect two precipitation pathways, convective and large-scale precipitation. For convective precipitation, MSE increases due to increased atmospheric moisture and warmer air temperatures in RunI (equation (6); r = 0.224). This is evident in Figure 8 where there is a direct relationship between MSE anomalies and surface soil temperature differences (a difference of 1 K in soil temperature at the surface corresponds to a 1 kJ kg^{-1} change in MSE). This soil moisture–convective precipitation feedback cycle is most important during the fringe winter months (April and October for the NGP region) within the coupled region. The winter land-atmosphere feedback also affects large-scale precipitation through warmer temperatures and increased evapotranspiration in the interactive run (RunI). Warmer temperatures decrease relative humidity at lower levels in the atmosphere (<700 mbar), corresponding to a decrease in fractional cloud cover. Due to the reduction in cloud cover, the autoconversion threshold decreases requiring less in-cloud water to produce large-scale precipitation (Figure 10). Additionally, increased evapotranspiration provides more moisture to the atmosphere. The higher moisture flux into the atmosphere further promotes large-scale precipitation higher in the atmosphere (>700 mbar). The large scale soil moisture–precipitation feedback occurs during transition months that are colder and have more large-scale precipitation (March and November for the NGP region).

[43] Regions where this feedback is valid are determined by the frequency and persistence of cold air masses. As a region transitions further into winter, the heat reservoir from the near-surface soil column (e.g., shallower than 50 cm) is drawn down and eventually extinguished. This terminates the land-atmosphere feedback, as seen at higher latitudes during DJF (Figures 6 and 8). This behavior is also reflected in the migrating behavior of the coupling region, which tends to be located slightly south of the surface freezing line. Therefore, the freezing line represents a time-evolving transition zone.

6. Conclusion

[44] This study outlines a winter land-atmosphere feedback mechanism that highlights the importance of the soil water phase and soil moisture–precipitation feedbacks throughout the seasonal cycle. We find that there are two distinct land-atmosphere coupling regimes present. The first coupling regime is the feedback traditionally observed during the summer, where an increase in soil moisture increases latent heat release, MSE in the atmosphere, and convective precipitation [e.g., *Pal et al.*, 2001, and references therein]. The RegCM-CLM reproduces this type of coupling regime as noted in GLACE over the Southern Plains during JJA. However, here we highlight a second, not previously discussed land-atmosphere coupling regime during the winter midlatitudes that is a function of soil water phase. This winter coupling regime is driven by the ability of soil moisture phase to control surface fluxes, which can create a set of feedbacks that influence convective and large-scale precipitation (Figures 9 and 11). As a result of this winter feedback, the land-atmosphere winter coupling regimes are located slightly south of the freezing line. In this respect, the freezing line may be regarded as a temporally

varying transition zone similar to the semiarid to moist transition zone discussed in *Guo et al.* [2006] for boreal summer.

[45] The results are discussed from the perspective of simulations performed by one regional climate model, RegCM-CLM. Prior land-atmosphere coupling studies with multiple models indicate that coupling strength can vary substantially between models [*Dirmeyer et al.*, 2006], therefore studies with other high-resolution models would further elucidate this mechanism and identify any inherent model biases that could affect the winter coupling strength and mechanism. Additionally, there are known biases in our simulation of temperature and precipitation (section 4.1), yet the model biases do not appear to track the coupling pattern. Therefore the proposed mechanism and the winter coupling are likely not artifacts of those specific model biases. However, the temperature and precipitation biases may enhance or dampen the coupling strength and affect the timing of the land-atmosphere feedbacks.

[46] The nature of the climate model experiment and fixed climatological soil water phase can lead to a deviation from the mean climate state where RunC develops atmospheric temperatures that are on average colder than the RunI simulations (e.g., Figures 6 and 7). Although the experiment design may represent a case that is not observed in the atmosphere, comparing RunC to RunI demonstrates the ability of the presence of soil ice to guide the atmosphere to a colder mean state and illustrates the winter land-atmosphere feedback. These limitations notwithstanding, the results in this paper present a seasonal perspective on land-atmosphere coupling and suggest a winter feedback triggered by the presence of soil ice.

[47] **Acknowledgments.** We thank the ICTP and its staff for supporting portions of the RegCM-CLM model development, and Sara Rauscher and three anonymous reviewers for helpful comments on the manuscript.

References

Betts, A. K. (2004), Understanding hydrometeorology using global models, *Bull. Am. Meteorol. Soc.*, *85*, 1673–1688, doi:10.1175/BAMS-85-11-1673.

Betts, A. K., and J. H. Ball (1995), The FIFE surface diurnal cycle climate, *J. Geophys. Res.*, *100*, 25,679–25,693.

Betts, A. K., J. H. Ball, A. C. M. Beljaars, M. J. Miller, and P. A. Viterbo (1996), The land surface–atmosphere interaction: A review based on observational and global modeling perspectives, *J. Geophys. Res.*, *101*, 7209–7225.

Bony, S., et al. (2006), How well do we understand and evaluate climate change feedback processes?, *J. Clim.*, *19*, 3445–3482.

Boone, A., V. Masson, T. Meyers, and J. Noilhan (2000), The influence of the inclusion of soil freezing on simulations by a soil-vegetation-atmosphere transfer scheme, *J. Appl. Meteorol.*, *39*, 1544–1569.

Collins, W. D., et al. (2006), The community climate system model version 3 (CCSM3), *J. Clim.*, *19*, 2122–2143.

Cosgrove, B. A., et al. (2003), Land surface model spin-up behavior in the North American Land Data Assimilation System (NLDAS), *J. Geophys. Res.*, *108*(D22), 8845, doi:10.1029/2002JD003316.

de la Torre, L., R. Nieto, M. Nogruerol, J. A. Anel, and L. Gimeno (2008), A climatology based on reanalysis of baroclinic developmental regions in the extratropical Northern Hemisphere, in *Trends and Directions in Climate Research*, edited by L. Gimeno et al., *Ann. N. Y. Acad. Sci.*, *1146*, 235–255.

Dirmeyer, P. A. (2001), An evaluation of the strength of land-atmosphere coupling, *J. Hydrometeorol.*, *2*, 329–344.

Dirmeyer, P. A. (2006), The hydrologic feedback pathway for land-climate coupling, *J. Hydrometeorol.*, *7*, 857–867.

Dirmeyer, P. A., R. D. Koster, and Z. C. Guo (2006), Do global models properly represent the feedback between land and atmosphere?, *J. Hydrometeorol.*, *7*, 1177–1198.

Duffy, P. B., R. W. Arritt, J. Coquard, W. Gutowski, J. Han, J. Iorio, J. Kim, L. R. Leung, J. Roads, and E. Zeledon (2006), Simulations of present and future climates in the western United States with four nested regional climate models, *J. Clim.*, *19*, 873–895.

Eltahir, E. A. B. (1998), A soil moisture rainfall feedback mechanism: 1. Theory and observations, *Water Resour. Res.*, *34*, 765–776.

Emanuel, K. A. (1995), On thermally direct circulations in moist atmospheres, *J. Atmos. Sci.*, *52*, 1529–1534.

Fennessy, M. J., and J. Shukla (1999), Impact of initial soil wetness on seasonal atmospheric prediction, *J. Clim.*, *12*, 3167–3180.

Findell, K. L., and E. A. B. Eltahir (1997), An analysis of the soil moisture–rainfall feedback, based on direct observations from Illinois, *Water Resour. Res.*, *33*, 725–735.

Findell, K. L., and E. A. B. Eltahir (2003), Atmospheric controls on soil moisture–boundary layer interactions, Part II: Feedbacks within the continental United States, *J. Hydrometeorol.*, *4*, 570–583.

Giorgi, F., and G. T. Bates (1989), The climatological skill of a regional model over complex terrain, *Mon. Weather Rev.*, *117*, 2325–2347.

Giorgi, F., and L. O. Mearns (1999), Introduction to special section: Regional climate modeling revisited, *J. Geophys. Res.*, *104*, 6335–6352.

Grell, G. A. (1993), Prognostic evaluation of assumptions used by cumulus parameterizations, *Mon. Weather Rev.*, *121*, 764–787.

Guo, Z. C., et al. (2006), GLACE – The Global Land-Atmosphere Coupling Experiment, part II: Analysis, *J. Hydrometeorol.*, *7*, 611–625.

Henry, H. A. L. (2008), Climate change and soil freezing dynamics: Historical trends and projected changes, *Clim. Change*, *87*, 421–434.

Isard, S. A., and R. J. Schaetzl (1998), Effects of winter weather conditions on soil freezing in southern Michigan, *Phys. Geogr.*, *19*, 71–94.

Kalnay, E., et al. (1996), The NCEP/NCAR 40 year reanalysis project, *Bull. Am. Meteorol. Soc.*, *77*, 437–471.

Kim, Y., and G. L. Wang (2007), Impact of initial soil moisture anomalies on subsequent precipitation over North America in the coupled land-atmosphere model CAM3-CLM3, *J. Hydrometeorol.*, *8*, 513–533.

Koster, R. D., P. A. Dirmeyer, A. N. Hahmann, R. Ijpelaar, L. Tyahla, P. Cox, and M. J. Suarez (2002), Comparing the degree of land-atmosphere interaction in four atmospheric general circulation models, *J. Hydrometeorol.*, *3*, 363–375.

Koster, R. D., et al. (2004), Regions of strong coupling between soil moisture and precipitation, *Science*, *305*, 1138–1140.

Koster, R. D., et al. (2006), GLACE – The Global Land-Atmosphere Coupling Experiment, part I: Overview, *J. Hydrometeorol.*, *7*, 590–610.

Lawrence, P. J., and T. N. Chase (2007), Representing a new MODIS consistent land surface in the Community Land Model (CLM 3.0), *J. Geophys. Res.*, *112*, G01023, doi:10.1029/2006JG000168.

Leung, L. R., Y. Qian, and X. D. Bian (2003), Hydroclimate of the western United States based on observations and regional climate simulation of 1981–2000, part I: Seasonal statistics, *J. Clim.*, *16*, 1892–1911.

Mitchell, T. D., and P. D. Jones (2005), An improved method of constructing a database of monthly climate observations and associated high-resolution grids, *Int. J. Climatol.*, *25*(6), 693–712.

Niu, G. Y., and Z. L. Yang (2006), Effects of frozen soil on snowmelt runoff and soil water storage at a continental scale, *J. Hydrometeorol.*, *7*, 937–952.

Oleson, K. W., et al. (2008), Improvements to the Community Land Model and their impact on the hydrological cycle, *J. Geophys. Res.*, *113*, G01021, doi:10.1029/2007JG000563.

Pal, J. S., and E. A. B. Eltahir (2001), Pathways relating soil moisture conditions to future summer rainfall within a model of the land-atmosphere system, *J. Clim.*, *14*, 1227–1242.

Pal, J. S., E. E. Small, and E. A. B. Eltahir (2000), Simulation of regional-scale water and energy budgets: Representation of subgrid cloud and precipitation processes within RegCM, *J. Geophys. Res.*, *105*, 29,579–29,594.

Pal, J. S., et al. (2007), Regional climate modeling for the developing world: The ICTP RegCM3 and RegCNET, *Bull. Am. Meteorol. Soc.*, *88*, 1395–1409, doi:10.1175/BAMS-88-9-1395.

Reynolds, R. W., N. A. Rayner, T. M. Smith, D. C. Stokes, and W. Q. Wang (2002), An improved in situ and satellite SST analysis for climate, *J. Clim.*, *15*, 1609–1625.

Schar, C., D. Luthi, U. Beyerle, and E. Heise (1999), The soil-precipitation feedback: A process study with a regional climate model, *J. Clim.*, *12*, 722–741.

Seneviratne, S. I., D. Luthi, M. Litschi, and C. Schar (2006), Land-atmosphere coupling and climate change in Europe, *Nature*, *443*, 205–209.

Sickmoller, M., R. Blender, and K. Fraedrich (2000), Observed winter cyclone tracks in the northern hemisphere in reanalyzed ECMWF data, *Q. J. R. Meteorol. Soc.*, *126*, 591–620.

Steiner, A. L., J. S. Pal, S. A. Rauscher, J. L. Bell, N. S. Diffenbaugh, A. Boone, L. C. Sloan, and F. Giorgi (2009), Land surface coupling in regional climate simulations of the West African monsoon, *Clim. Dyn.*, *33*, 869–892.

Viterbo, P., A. Beljaars, J. F. Mahfouf, and J. Teixeira (1999), The representation of soil moisture freezing and its impact on the stable boundary layer, *Q. J. R. Meteorol. Soc.*, *125*, 2401–2426.

Walker, M. D., and N. S. Diffenbaugh (2009), Evaluation of high-resolution simulations of daily-scale temperature and precipitation over the United States, *Clim. Dyn.*, *33*, 1131–1147.

Wang, S. Y., R. R. Gillies, E. S. Takle, and W. J. Gutowski (2009), Evaluation of precipitation in the Intermountain Region as simulated by the NARCCAP regional climate models, *Geophys. Res. Lett.*, *36*, L11704, doi:10.1029/2009GL037930.

Wu, W. R., R. E. Dickinson, H. Wang, Y. Q. Liu, and M. Shaikh (2007), Covariabilities of spring soil moisture and summertime United States precipitation in a climate simulation, *Int. J. Climatol.*, *27*, 429–438.

Yang, F. L., A. Kumar, W. Q. Wang, H. M. H. Juang, and M. Kanamitsu (2001), Snow-albedo feedback and seasonal climate variability over North America, *J. Clim.*, *14*, 4245–4248.

Zhang, H., and C. S. Frederiksen (2003), Local and nonlocal impacts of soil moisture initialization on AGCM seasonal forecasts: A model sensitivity study, *J. Clim.*, *16*, 2117–2137.

Zhang, J. Y., W. C. Wang, and L. R. Leung (2008a), Contribution of land-atmosphere coupling to summer climate variability over the contiguous United States, *J. Geophys. Res.*, *113*, D22109, doi:10.1029/2008JD010136.

Zhang, J. Y., W. C. Wang, and J. F. Wei (2008b), Assessing land-atmosphere coupling using soil moisture from the Global Land Data Assimilation System and observational precipitation, *J. Geophys. Res.*, *113*, D17119, doi:10.1029/2008JD009807.

A. L. Steiner and A. B. Tawfik, Department of Atmospheric, Oceanic, and Space Sciences, University of Michigan, Space Research Building, 2455 Hayward St., Ann Arbor, MI 48109-2143, USA. (abtawfik@umich.edu)